

## Article

# Topology Optimization Based Parametric Design of Balloon Borne Telescope's Primary Mirror

Fengchang Liu <sup>1,2,\*</sup>, Wei Li <sup>1,2,\*</sup>, Weiguo Zhao <sup>1</sup>, Haibo Zhao <sup>1</sup>, Guanyu Lin <sup>1</sup> and Xiaodong Wang <sup>1</sup>

<sup>1</sup> Changchun Institute of Optics, Fine Mechanics and Physics, Chinese Academy of Sciences, Changchun 130033, China; z-w-g@163.com (W.Z.); zhaohaibo07@sina.com (H.Z.); linguanyu7607266@sohu.com (G.L.); wangxd@ciomp.ac.cn (X.W.)

<sup>2</sup> Center of Materials Science and Optoelectronics Engineering, University of Chinese Academy of Sciences, Beijing 100049, China

\* Correspondence: liufengchang17@mails.ucas.edu.cn (F.L.); leew2006@ciomp.ac.cn (W.L.)

**Abstract:** For balloon-borne telescopes, the primary mirror is the most important optical element, but designing a primary mirror with an excellent overall performance is a challenge. To comprehensively consider the contradictory objectives of the root mean square (RMS) surface error under gravity in the X and Z directions, the mass and fundamental frequency of the primary mirror, a parametric primary mirror design using the compromise programming method based on topology optimization is proposed. The parametric design of the compromise programming method based on topology optimization is used to find the optimal solution for X-direction RMS (RMS<sub>x</sub>), Z-direction RMS (RMS<sub>z</sub>), mass, and fundamental frequency. Compared with the initial primary mirror structure designed according to traditional experience, the overall performance is improved. Results show that the respective mass of the primary mirror, the RMS<sub>x</sub> and the RMS<sub>z</sub> decreased by 8.5%, 14.3% and 10.5% compared to those before optimization. Comprehensive consideration can prove the effectiveness of parametric design based on the topology optimization of the primary mirror. This method provides a reference for the design of other primary mirrors for balloon-borne telescope and space cameras.

**Keywords:** near-space; primary mirror; topology optimization; parametric design; compromise programming method



**Citation:** Liu, F.; Li, W.; Zhao, W.; Zhao, H.; Lin, G.; Wang, X. Topology Optimization Based Parametric Design of Balloon Borne Telescope's Primary Mirror. *Appl. Sci.* **2021**, *11*, 5077. <https://doi.org/10.3390/app11115077>

Academic Editors: Jérôme Morio, Mathieu Balesdent and Loïc Brevault

Received: 14 April 2021

Accepted: 25 May 2021

Published: 30 May 2021

**Publisher's Note:** MDPI stays neutral with regard to jurisdictional claims in published maps and institutional affiliations.



**Copyright:** © 2021 by the authors. Licensee MDPI, Basel, Switzerland. This article is an open access article distributed under the terms and conditions of the Creative Commons Attribution (CC BY) license (<https://creativecommons.org/licenses/by/4.0/>).

## 1. Introduction

Near-space, also called suborbital space, is the airspace 20–100 km away from the Earth's surface [1,2]. With the increasingly fierce competition in space exploration, scientists have turned their attention to near space. Near-space exploration has a bright future in the fields of military strategy and scientific observation. European and American technologies are relatively mature and have numerous successful payload observation missions for balloon-borne telescopes, and Japan developed the FUJIN telescope for planetary observations. These tasks are mainly for multidisciplinary observations (astrophysics, heliophysics, and planetary and earth science), such as the ball-borne large-aperture submillimeter telescope [3,4], Terahertz Observatory (STO) [5], Sunrise [6], and the balloon-borne telescope [7], which have obtained observational data in planetary physics and solar physics, providing some effective bases for scientists to study planets and solar systems. Near-space exploration has more possibilities than space exploration, has the advantages of low cost and fast response, and can be recyclable multiple times. Compared with the ground-based large-diameter telescope, developing the balloon-borne telescope has an important scientific significance because reducing the atmospheric impact can detect the ultraviolet, gamma ray, and other wave bands absorbed by the atmosphere. As the key optical element of the telescope, the performance of the primary mirror affects the imaging quality to a certain extent. Therefore, the design of a primary mirror with high stiffness, low mass, and

high stability is the near-space objective. The design of a balloon-borne telescope's primary mirror faces two main challenges: the root mean square (RMS) (RMS with piston, tilt, and focus Zernike terms removed) must satisfy the requirements under the effect of changing gravity, and the mass of the primary mirror is restricted by the balloon limitation.

The primary mirror is the most important and sensitive element of an optical telescope. The design of the primary mirror mainly considers surface shape accuracy, mass and fundamental frequency. Significant research on the design and optimization of the primary mirror has been reported. Barthol et al. presented a study of the Sunrise telescope for observing the sun. This telescope has a 1000 mm Zerodur primary mirror, which has a three-point support at the back, an open-back triangular lightweight cell (lightweight cell means the space between ribs) [8]. Catanzaro et al. presented a study of the Gondola for High Altitude Planetary Science (GHAPS) that adopted triangular lightweight cells and an open-back structure. The mass of the primary mirror is 40 kg, and its supporting structure has a composite support form of lateral rods and an 18-point whiffletree structure at the back. The components meet the design requirements [9]. In addition to the traditional empirical design of the primary mirror, topology optimization methods are also widely used in the primary mirror design process. Park et al. made a topology optimization design for the primary mirror by considering the gravity in the optical axis direction and the polishing stress, achieving an RMS with a better performance than that of the traditional hexagonal lightweight structure [10]. Hu et al. took the minimum compliance of the mirror as the objective to constrain the mass of the topological optimization design of the mirror. Compared with that of the traditional hexagonal lightweight mirror, the RMS decreased by 62.5% [11]. Qu et al. presented a method that combines topology optimization with a multi-objective function with parametric optimization. The new configuration design shows obvious superiority over two types of traditional lightweight configurations [12]. Li et al. designed a  $\phi 760$  mm lightweight mirror and a flexible support structure. Under the condition of constraining its mass, topology optimization maximizes the stiffness of the mirror. The flexible structure was designed and tested to verify that the primary mirror assembly satisfies the surface shape requirements of  $\lambda/50$  nm under various working conditions [13]. In addition, the topology and parametric-optimization-based lightweight design of a space reflective mirror were studied by Liu et al. [14]. Jiang and Zhou used the topology optimization method to solve the axial support position sensitivity problem of the primary mirror. After topology optimization, not only was the sensitivity of the axial support position reduced, but the lightweight ratio and the fundamental frequency were also improved [15]. In recent years, a multi-objective topology optimization method based on the compromise programming method has been widely used by researchers. Xiao et al. optimized the steel wheel using the compromise programming method, which is employed to define the objectives of multi-objective and multi-stiffness topology optimizations; the optimized wheel decreased mass was reduced by 4.7% [16]. For Qiao et al., on the basis of obtaining the weight coefficients, the compromise planning method was used to optimize the topology, and the stiffness and fundamental frequency of the optimized frame structure were significantly improved [17].

In this paper, the parametric design of the primary mirror using the compromise programming method based on topology optimization is presented. The multi-objective topology optimization design of the primary mirror of the shell element was made using Optistruct. Considering the continuous change of gravity in the observation, the weighted compliance of the primary mirror under different observation angles was taken as the objective to constrain its mass and fundamental frequency. The base structure approach and the manufacturing constraints were used to improve the manufacturability of the primary mirror. The results of the topology optimization provide a different material distribution for each stiffener (rib). Therefore, the ribs can be easily grouped based on the topology optimization results. To solve the conflicting goals for the RMS, the mass, and the fundamental frequency, the compromise programming method was used for parametric design to find a compromise solution and realize automatic parameterization update

iteration with Isight to improve the parameterization efficiency and save in optimization time. The mass and RMSz of the primary mirror after parametric design were improved compared with those of the initial structure. Therefore, this optimization method can solve the contradictory multi-objective problem. The method can be applied to a balloon-borne telescope's primary mirror design in the future. The balloon-borne telescope mission is in the manufacturing phase and is expected to be launched in 2022.

## 2. Optimization Design of the Primary Mirror

### 2.1. Optical System

The balloon-borne telescope adopts the Ritchey–Chrétien system, which can obtain an angular resolution of 0.5". The optical system is shown in Figure 1. The distance between the primary mirror and the secondary mirror is 957 mm, and the working spectrum range of ultraviolet light to visible light is 280–680 nm. The distance of the entire optical system is 1500 mm. The aperture of the primary mirror is 800 mm, and the radius of curvature is 2800 mm [18].

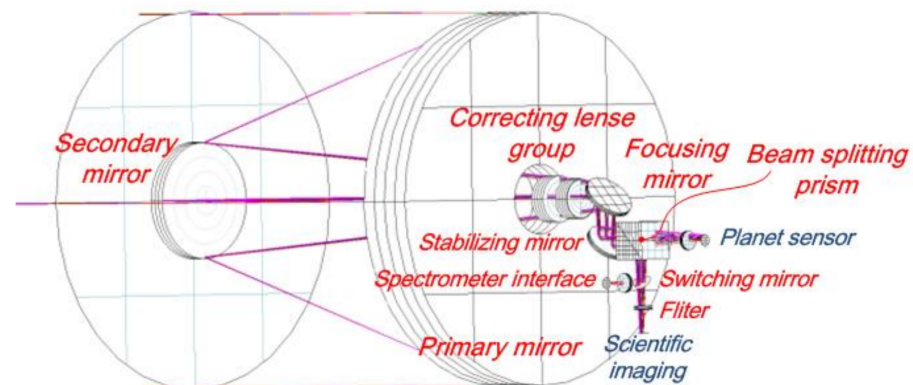


Figure 1. Optical system.

### 2.2. Initial Model Design of Primary Design

The balloon-borne telescope is affected by gravity. The premise to ensure the RMS of the primary mirror is that the mirror body has sufficient stiffness to resist gravity deformation. Meanwhile, referring to the design of GHAPS, the composite support mode of the back and peripheral supports is adopted to ensure the RMS during the observation process, so the whiffletree and A-frame structure are used to realize kinematic spatial positioning [19]. The thickness ratio, the support points, and the lightweight structure are usually considered in the design of the primary mirror. According to Roberts et al.'s research, empirical Formula (1) is given; the minimum number of back support points can be calculated by empirical Formula (2) given by Hall [20].

$$\delta = \frac{3\rho gr^4}{16Et^2} = \frac{3\rho gdr^2D^2}{256E} \quad (1)$$

$$N = \left( \frac{1.5r^2}{t} \right) \left( \frac{\rho}{E\delta'} \right)^{0.5} \quad (2)$$

where  $\delta$  is the maximum self-weight deformation of the mirror surface,  $\mu\text{m}$ ;  $\rho$  is the density of the primary mirror,  $\text{kg}/\text{m}^3$ ;  $g$ : the acceleration of gravity,  $\text{g}/\text{s}^2$ ;  $r$  is the radius of primary mirror ( $r = D/2$ ),  $\text{m}$ ;  $E$  is the elastic modulus of the primary mirror,  $\text{Gpa}$ ;  $t$  is the thickness of the primary mirror,  $\text{m}$ ; and  $\delta'$  is the surface PV value,  $\text{nm}$ . According to the error distribution and the relationship between the PV and the RMS values, the PV value is no more than 30 nm.

The balloon-borne telescope primary mirror assembly adopts passive support, which consists of a 6-point axial support and three A-frame lateral supports. The passive support employs a 6-point whiffletree for axial constraint (piston, tip, and tilt DOFs) and a set of

three A-frame supports for lateral support (two in-plane and one clocking DOFs). The common lightweight cells of the mirror include triangular, fan, square, and hexagonal structures. The triangle lightweight structure can provide better specific stiffness, stability, and optical quality than the other structures. Considering that the distribution of ribs very near the center hole will increase the difficulty of processing, the lightweight structure of the triangle and local central sector is adopted to design the primary mirror. A SiC primary mirror with a partially closed back was designed. The advantages of the partially closed back design include high mirror flexural rigidity relative to open-back designs and fabrication simplicity relative to built-up configurations. However, a partially closed back structure tends to have a much slower thermal response time than an open-back structure. To reduce the deformation of the edge of the primary mirror, radial ribs are arranged at the edge. The aperture of the primary mirror is 800 mm. Considering the edge effect during processing, the aperture of the primary mirror is 816 mm, the inner ring diameter is 722 mm, the diameter of the back support hole distribution circle is 519 mm, the diameter of the central hole is 160 mm, the diameter of six back support is 30 mm, the thickness of the mirror face is 6 mm, the thickness of the back face is 8 mm, and the thickness of the other ribs is 5 mm. Considering the commonly used materials of the primary mirror, the comprehensive performance of third-generation mirror material RB-SiC is better than that of glass-ceramic and Be, and Changchun Institute of Optics, Fine Mechanics and Physics has an independent SiC mirror-manufacturing technology, which is in the leading position in China. Thus, the RB-SiC material is used for the primary mirror. The material properties are shown in Table 1. The mass of the initial primary mirror is 33.8 kg, and a 75.8% lightweight ratio is achieved. Figure 2 shows primary mirror assembly showing the lateral support, axial support, mirror body, the back support holes, and basic dimensions.

**Table 1.** RB-SiC Material Property.

Material	E (Gpa)	$\rho$ ( $10^{-9}$ t/mm <sup>3</sup> )	$\mu$
RB-SiC	330	3.05	0.25

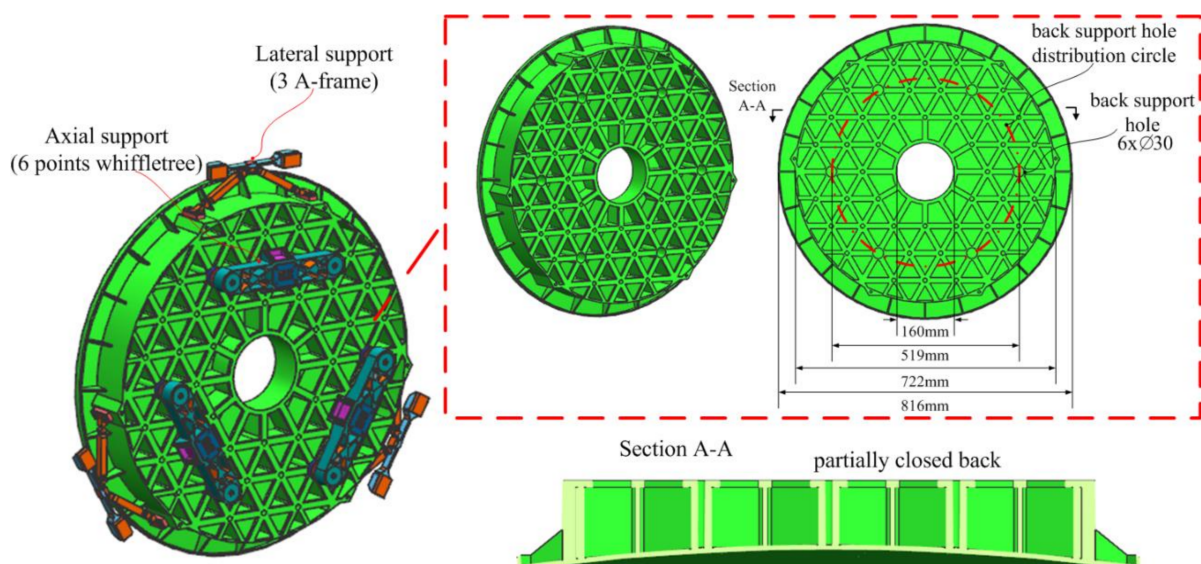


**Figure 2.** Primary mirror assembly showing the lateral support, axial support, mirror body, the back support holes, and basic dimensions.

The primary mirror of the balloon-borne telescope must ensure good imaging quality. The actual mirror surface accuracy index can be obtained by root mean square of mirror surface accuracy in mechanical stability tolerance and processing and assembly tolerance, but there is overlap between them. Therefore, in the actual design and development

process, referring to the optical design tolerance allocation requirements, the RMS values of the surface shape error of the mirror parallel to the X and Z axes under gravity should not exceed  $\lambda/60$  nm (where  $\lambda = 632.8$  nm represents the wavelength of visible light). In addition, to ensure the stability of the primary mirror assembly, the fundamental frequency should not be lower than 2100 Hz. Given the mass limitation of balloon and launch costs, the mass of the primary mirror assembly does not exceed 100 kg. For primary mirror assembly, including primary mirror, flexure supports, and primary mirror chamber, the mass of the primary mirror should be less than 32.5 kg. The design requirements of the primary mirror are shown in Table 2.

**Table 2.** Design requirements of primary mirror.

Primary Mirror	RMSx (nm)	RMSz (nm)	M (kg)	f1 (Hz)
Index	$\leq \lambda/60$	$\leq \lambda/60$	$\leq 32.5$	$\geq 2100$

### 2.3. Topology Optimization of Primary Mirror

Topology optimization can optimize the material distribution or obtain the best force transmission path in the design domain, which can play a strong basis for the classification of the primary mirror ribs. Compared with the traditional optimization based on the location and experience, it can improve the RMS values of the surface shape error of the primary mirror and reduce the mass. In this study, a topology optimization method with a multi-objective function is introduced for the primary mirror design using Optistruct. To reduce the calculation time, improve the optimization efficiency, and increase the flexibility of variables, the primary mirror finite-element model is established with linear shell elements. As shown in Figure 3, the topology optimization model comprises a design domain and a non-design domain. The mirror face, the six back support holes, and the bonding surface of the peripheral support are assigned to the non-design domain, and the rest to the design domain. The total number of elements is 41,946, and the total number of nodes is 38,706. The distribution of the material is determined based on SIMP to find the best force transmission path [21,22]. The basic idea is to assume a material element that has variable relative density  $\rho$  between 0 and 1. The red part represents the elements with a density of 1, and the blue part represents elements with a density near zero. The nearer the density to 1, the higher the material importance is [23]. To avoid more intermediate density units, the mathematical model introduces penalty factor  $r$ , and the assumed function relationship between density and the elastic modulus of the material is as follows:

$$E_i = (\rho_i)^r E_0 \quad i = 1, 2, \dots, n. \quad (3)$$

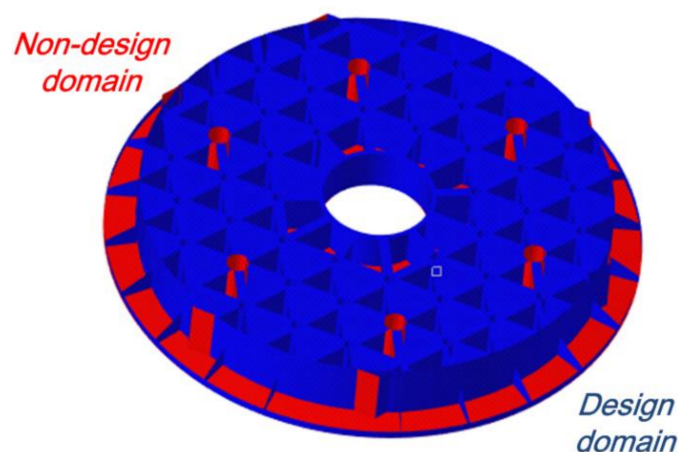


**Figure 3.** Design domain and non-design domain.

Here,  $n$  is the total number of the discrete finite elements.  $E_i$  is the material characteristic of the design unit, that is, the elastic modulus;  $\rho_i$  is the density of the material;  $E_0$  is the initial value of the elastic modulus of the material;  $r$  is the penalty factor (in order to obtain a clear 0–1 design, take 3); and the topology optimization model can be expressed as follows:

$$\text{Find} \quad X = (\rho_1, \rho_2, \dots, \rho_n)^T \tag{4}$$

Optimization objective

$$\text{Min} \quad C_w = \alpha C_{0^\circ} + \beta C_{30^\circ} + \chi C_{60^\circ} + \gamma C_{90^\circ} \tag{5}$$

Subject to

$$\delta \leq \bar{U} \tag{6}$$

$$\text{mass} \leq M \tag{7}$$

$$G_k(X) = 0 \tag{8}$$

$$KU = F \tag{9}$$

$$0 < \rho_{\min} \leq \rho_i \leq 1 \quad (i = 1, 2, \dots, n) \tag{10}$$

The optimization goal is that the weighted compliance of the telescope is the minimum at the observation angles of  $0^\circ$ ,  $30^\circ$ ,  $60^\circ$ , and  $90^\circ$ , that is, the stiffness is the maximum. (The stiffness under each observation angle is very important, so take  $\alpha = \beta = \chi = \gamma = 0.25$ ), which can improve the RMS values of the surface shape error of the primary mirror.  $\delta$  is the displacement of the node of mirror face ( $\bar{U}$ : the upper line of the displacement of the primary mirror node along the optical axis is 30 nm). According to Kim’s research [24], constrained mirror face deformation can obtain better surface figure RMS.  $M$  is the upper quality limit of the design index of the primary mirror, a pattern grouping constraint is imposed in the design domain to generate a central symmetric configuration,  $G_k(X)$  represents the  $120^\circ$  circumferential cyclic symmetry constraint between the  $k$ th elements of the primary mirror, and  $\rho_{\min}$  is the lower limit of the relative density of the element set to avoid the singularity of the stiffness matrix during the optimization process.

The weighted compliance of the observation angle gravity is used as the topology optimization objective, and sensitivity analysis is performed on the weighted structural compliance. When a rigid body rotates around an axis by a micro angle, the direction of the angular displacement vector follows that axis. Therefore, Equations (1)–(3) can be transformed into

$$\frac{\partial C_w}{\partial \rho_i} = \alpha \left[ \left( F_{0^\circ}^T - \hat{U}_{0^\circ}^T K \right) \frac{\partial U_{0^\circ}}{\partial \rho_i} - U_{0^\circ}^T \frac{\partial K}{\partial \rho_i} U_{0^\circ} \right] + \beta \left[ \left( F_{30^\circ}^T - \hat{U}_{30^\circ}^T K \right) \frac{\partial U_{30^\circ}}{\partial \rho_i} - U_{30^\circ}^T \frac{\partial K}{\partial \rho_i} U_{30^\circ} \right] + \chi \left[ \left( F_{60^\circ}^T - \hat{U}_{60^\circ}^T K \right) \frac{\partial U_{60^\circ}}{\partial \rho_i} - U_{60^\circ}^T \frac{\partial K}{\partial \rho_i} U_{60^\circ} \right] + \gamma \left[ \left( F_{90^\circ}^T - \hat{U}_{90^\circ}^T K \right) \frac{\partial U_{90^\circ}}{\partial \rho_i} - U_{90^\circ}^T \frac{\partial K}{\partial \rho_i} U_{90^\circ} \right] \tag{11}$$

$KU = F$  according to the symmetry of  $K$ , and the adjoint equations  $K\hat{U} = F$  and  $\hat{U} = U$  are established. Formula (11) can be expressed as follows:

$$\frac{\partial C_w}{\partial \rho_i} = -\alpha \left[ U_{0^\circ}^T \frac{\partial K}{\partial \rho_i} U_{0^\circ} \right] - \beta \left[ U_{30^\circ}^T \frac{\partial K}{\partial \rho_i} U_{30^\circ} \right] - \chi \left[ U_{60^\circ}^T \frac{\partial K}{\partial \rho_i} U_{60^\circ} \right] - \gamma \left[ U_{90^\circ}^T \frac{\partial K}{\partial \rho_i} U_{90^\circ} \right] \tag{12}$$

The topology optimization results tend to converge after 179 iterations; Figure 4 shows the material distribution results of the topology optimization. The ribs can be easily grouped based on the topology optimization results. The grouping of the primary mirror variables is shown in Figure 5a,b. Considering that many parameters must be considered during the parametric design based on compromise planning theory, sensitivity analysis is performed on the primary mirror to improve the efficiency of the parametric design.

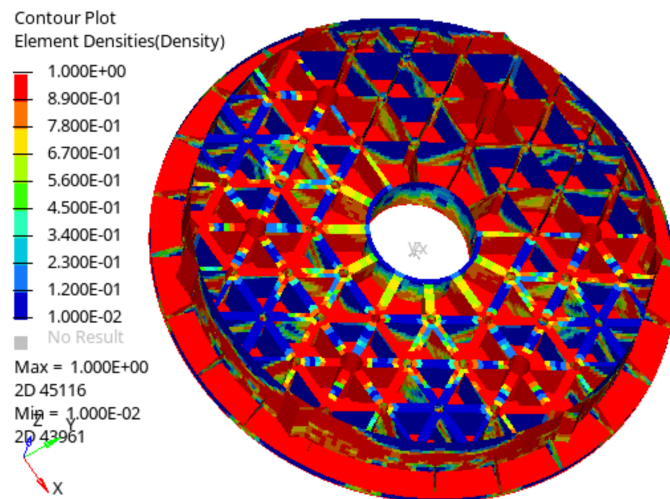


Figure 4. Material distribution result of the topology optimization.

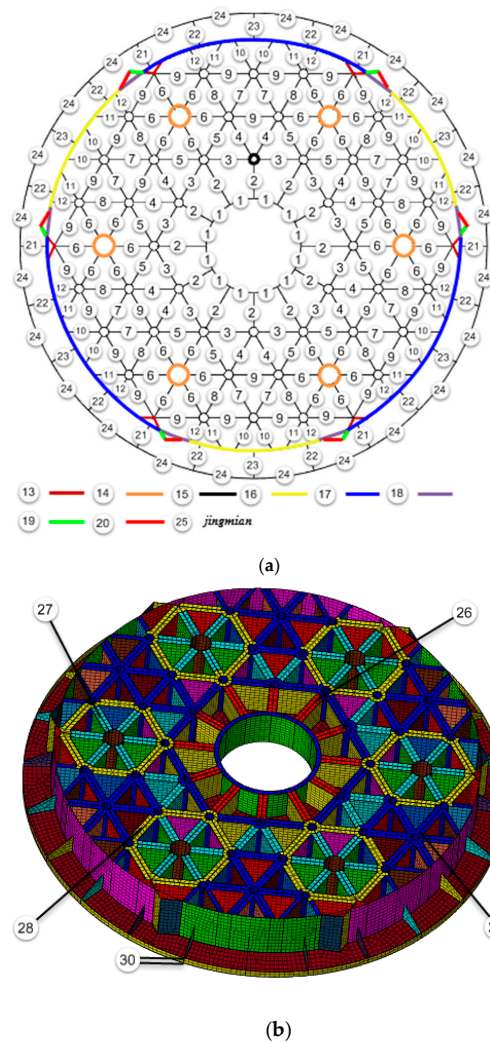


Figure 5. Grouping of primary mirror ribs based on topology optimization. (a) the mirror face and each ribs group number (b) the back face and edge rib height group number.

### 3. Parametric Design of Primary Mirror

The parametric design of the primary mirror of the balloon-borne telescope is a multi-objective optimization problem. The RMS values of the surface shape error, and

the fundamental frequency and the mass should be considered in the parametric design of the primary mirror. The RMS value of the surface shape error contradicts with the fundamental frequency and the mass, so achieving the optimum values at the same time is nearly impossible. Moreover, the fundamental frequency, the RMS, and the mass are measured in different ways. Therefore, we hope to transform this multi-objective problem into a single problem for processing. Thus, the compromise programming method is used to find a compromise solution to multi-objective optimization.

### 3.1. Theory of Compromise Programming Method

Using the compromise programming method to set the optimization function, the maximum value of any function can be transformed into the minimum value of the negative function, so all multi-objective optimization problems can be expressed as

$$\begin{cases} \text{find } x = (x_1, x_2, \dots, x_m) \\ \text{min } f_i(x), i = 1, 2, \dots, n \\ \text{s.t. } x \in X \end{cases} \quad (13)$$

where  $x$  is the optimization variable,  $m$  is the number of optimization variables,  $f_i(x)$  is the  $i$ th sub-objective function,  $n (n \geq 2, n \in N)$  is the total number of objective functions, and  $X$  is the constraint set of the optimization variables. Assuming that the ideal solution of the objective function of multi-objective optimization (the optimal solution in single-objective optimization) is  $a^{\min} = \{a_1^{\min}, a_2^{\min}, \dots, a_n^{\min}\}$ , then the compromise solution of the multi-objective optimization problem is the vector with minimum distance  $X$  from the ideal solution [25]. In this case, the multi-objective optimization problem can be transformed into a single-objective optimization problem, and the objective function can be expressed as:

$$\min F(t) = \left\{ \sum_{k=1}^n w_k^p [f_k(t) - a_k^{\min}]^p \right\}^{\frac{1}{p}} \quad (14)$$

where  $w_k$  is the weight ratio of the  $k$ th objective,  $p$  is the distance index, and the meaning of the objective function is different when  $p$  takes different values:

- (1) When  $p = 1$ , the meaning of the objective function is the sum of the ideal solution.
- (2) When  $1 < p < \infty$ , the meaning of the objective function is the weighted geometric distance from the ideal solution. Specifically, when  $p = 2$ , the objective function is the Euclidean distance.
- (3) When  $p = \infty$ , the meaning of the objective function is the Chebyshev distance, which is the maximum weighted distance.

When multi-objective optimization problems with different measurement methods exist, the absolute distance between the compromise solution of the objective function and its ideal solution can be transformed into a relative distance, and the objectives of different measurement methods can be compared to achieve the goal of a single-objective optimization problem [26,27].

$$\min F(t) = \left\{ \sum_{k=1}^n w_k^p \left[ \frac{f_k(t) - a_k^{\min}}{a_k^{\max} - a_k^{\min}} \right]^p \right\}^{\frac{1}{p}} \quad (15)$$

where  $a_k^{\max}$  and  $a_k^{\min}$  are the maximum and minimum values of each objective under its boundary conditions.

Using the theory of the compromise programming method, the parametric mathematical model of the primary mirror in near-space is expressed as formula (16).

$$\min F(t) = \left\{ w_x^2 \left[ \frac{R_x(t) - R_x^{\min}}{R_x^{\max} - R_x^{\min}} \right]^2 + w_z^2 \left[ \frac{R_z(t) - R_z^{\min}}{R_z^{\max} - R_z^{\min}} \right]^2 + w_m^2 \left[ \frac{m(t) - m^{\min}}{m^{\max} - m^{\min}} \right]^2 + w_f^2 \left[ \frac{f(t) - f^{\min}}{f^{\max} - f^{\min}} \right]^2 \right\}^{\frac{1}{2}} \quad (16)$$

where  $R_z(t)$  and  $R_x(t)$  are the mirror surface root mean squares caused by gravity in the Z and X directions, respectively;  $R_{\min}$  is the minimum value of the RMS under each working condition;  $R_{\max}$  is the maximum value of the RMS under each working condition;  $m(t)$  is the mass of the primary mirror;  $m_{\min}$  and  $m_{\max}$  are the minimum and maximum values of the mass respectively;  $f(t)$  is the fundamental frequency of the primary mirror;  $f_{\min}$  and  $f_{\max}$  are the minimum and maximum fundamental frequencies, respectively; and  $w$  is the weight of each optimization sub-objective. The weight factor is defined according to the importance of each parameter to the primary mirror. In order to reduce the cost of flight and the difficulty of balloon manufacturing, the mass of the primary mirror is as low as possible. Considering the differences in the deformation of the mirror under gravity parallel to the optical axis and perpendicular to the optical axis, the corresponding weight factors were set to 0.2, 0.3, 0.3, and 0.2, respectively.

The optimization algorithm is used to find the maximum and minimum values of each parameter to establish the compromise programming method mathematical model. After 501 optimization iterations, the maximum and minimum values of the primary mirror parameters were obtained. The objective function of parametric design is shown in Formula (17).

$$\min F(t) = \left\{ 0.2^2 \left[ \frac{R_x(t) - 1.647e^{-6}}{2.977e^{-6} - 1.647e^{-6}} \right]^2 + 0.3^2 \left[ \frac{R_z(t) - 4.684e^{-6}}{7.234e^{-6} - 4.684e^{-6}} \right]^2 + 0.3^2 \left[ \frac{m(t) - 0.029}{0.04069 - 0.029} \right]^2 + 0.2^2 \left[ \frac{f(t) - 2002.4}{2437 - 2002.4} \right]^2 \right\}^{\frac{1}{2}} \quad (17)$$

### 3.2. Sensitivity Analysis of Primary Mirror Parameters

Sensitivity analysis refers to the extent to which the changes in structural design parameters affect the performance of the objective function. The design of experiments (DoE) studies the relationship and trend between input and output parameters. This study has many parameters, and DoE can improve efficiency.  $F(t)$  is selected as the objective function of the sensitivity analysis. DoE results usually provide an approximate model between the input factors ( $X_i$ ) and the output response ( $Y$ ) in the form of a lower-order polynomial. In formula (18), the magnitudes of the coefficients in this equation reflect the strength of the  $X_i$  effects of factors on model output response  $Y$ . Each factor contains three levels. On the basis of orthogonal arrays ( $L_{81}$ ), this method is an efficient, fast, and economical experimental design method. This method has the advantages of balanced collocation of factor level and uniform distribution of data points, which greatly reduces the number of experimental analyses [28–30].

$$Y = C_0 + \sum_{i=1}^m C_i X_i + \sum_{i=1, j=1}^m C_{ij} X_i X_j \quad (18)$$

As shown in Figure 6, according to the sensitivity analysis of each parameter to  $F(t)$ , 22 parameters, namely ribs1, ribs2, ribs3, ribs4, ribs5, ribs6, ribs7, ribs8, ribs9, ribs10, ribs11, ribs12, ribs13, ribs14, ribs16, ribs17, ribs18, ribs20, ribs21, ribs25, ribs26 and ribs29, which have great contributions, are taken as the variables of the parametric design.

### 3.3. Parametric Design of Primary Mirror

Given the automatic parametric design, this study adopts the Isight software, which combines Hypermesh, Optistruct, and SigFit. The parametric design can find the global optimal solution, while automatic update iterations improve the optimization efficiency. The flow chart of the parametric design is shown in Figure 7. On the basis of the sensitivity analysis, 22 variables were selected for the parametric design. Considering the manufacturing capability of the mirror, the minimum thickness of primary mirror ribs is 3 mm, so the domain of rib26 and rib29 variable is 6–10 mm, and the domain of the rest of ribs variable is 3–8 mm. The parameterized model aims to obtain the minimum  $F(t)$  while constraining the mass of the primary mirror and the fundamental frequency. The parametric design mathematical model is shown in formula (19).

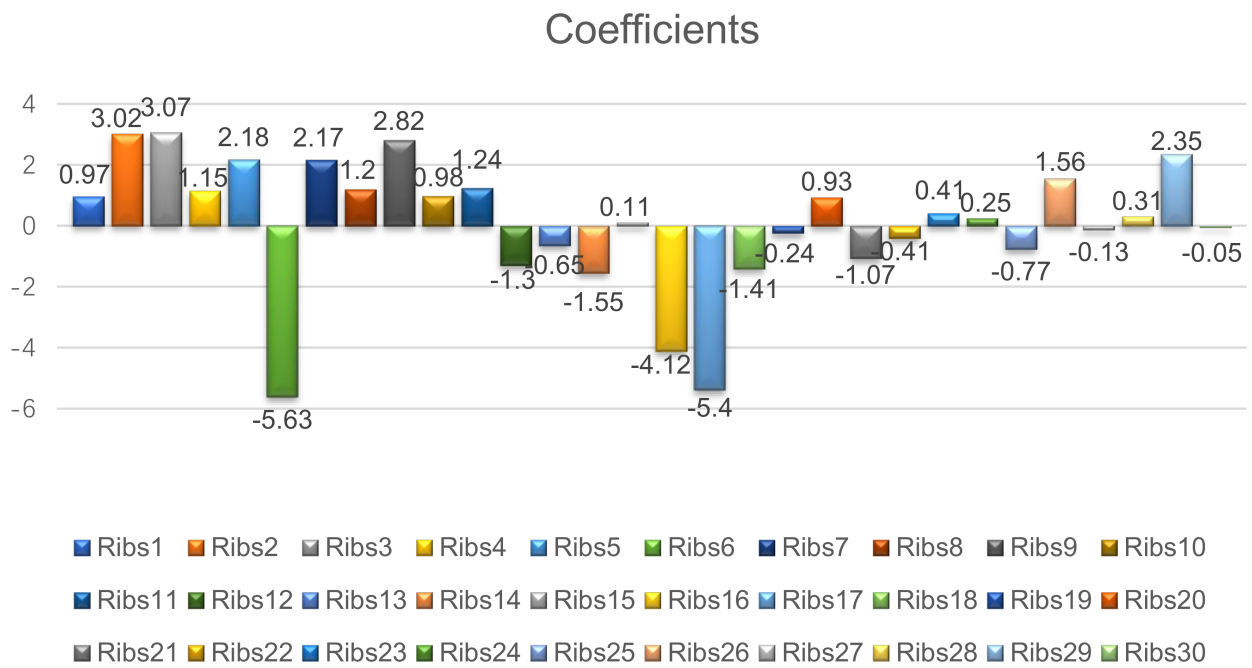


Figure 6. Contributions of the design parameters to the F(t).

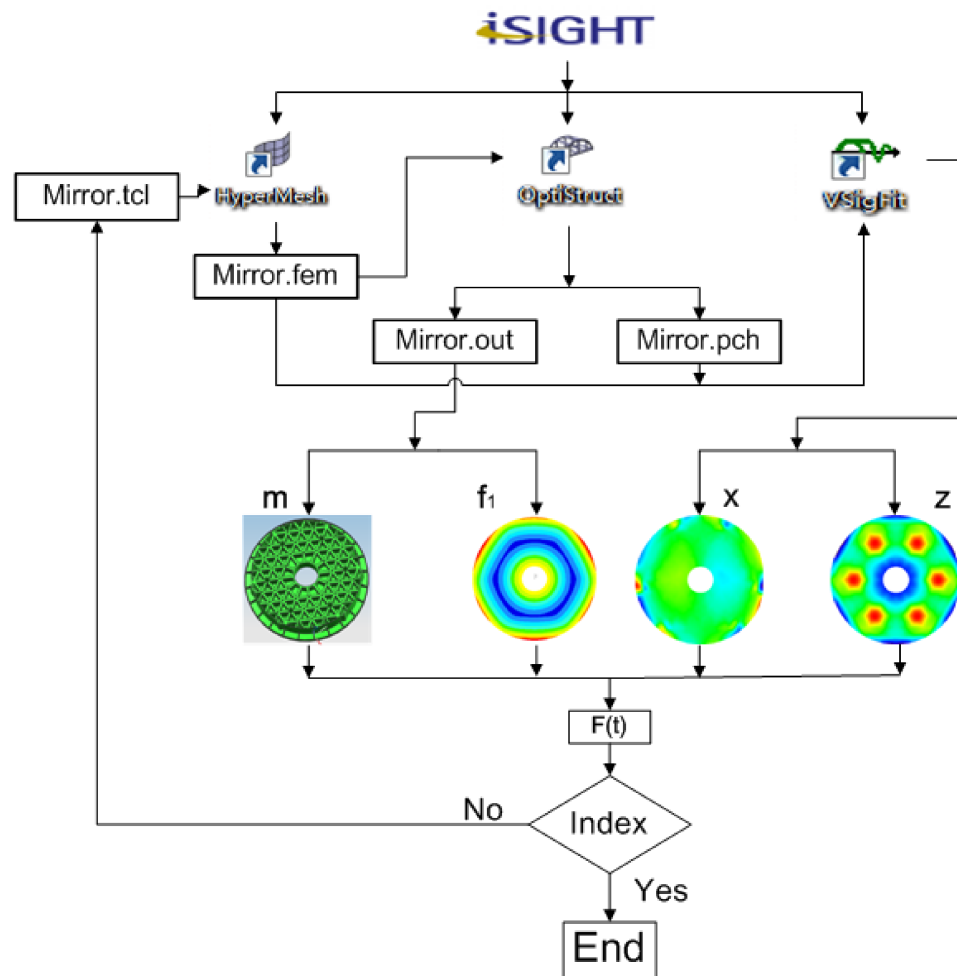


Figure 7. Flow chart of the parametric design of the primary mirror.

Parametric design mathematical model:

$$\begin{aligned}
 & \text{Find } t = (t_1, t_2, t_3, t_4, t_5, t_6, t_7, t_8, t_9, t_{10}, t_{11}, t_{12}, t_{13}, t_{14}, t_{16}, t_{17}, t_{18}, t_{20}, t_{21}, t_{25}, t_{26}, t_{29})^T \\
 \min F(t) = & \left\{ \begin{aligned} & 0.2^2 \left[ \frac{R_x(t) - 1.647e^{-6}}{2.977e^{-6} - 1.647e^{-6}} \right]^2 + 0.3^2 \left[ \frac{R_z(t) - 4.684e^{-6}}{7.234e^{-6} - 4.684e^{-6}} \right]^2 \\ & + 0.3^2 \left[ \frac{m(t) - 0.029}{0.04069 - 0.029} \right]^2 + 0.2^2 \left[ \frac{f(t) - 2002.4}{2437 - 2002.4} \right]^2 \end{aligned} \right\}^{\frac{1}{2}} \\
 & \text{s.t.} \\
 & \quad \text{mass} \leq M \\
 & \quad f_1 \geq \bar{f}_1 \\
 & \quad t_{i\_low} \leq t_i \leq t_{i\_up} \quad i = 1, 2, \dots, n
 \end{aligned} \tag{19}$$

The multi-island genetic algorithm is used to optimize the design of the compromise objective function. The multi-island genetic algorithm has better global solving ability and computational efficiency than the traditional genetic algorithm [31]. The optimized results of each variable are shown in Table 3. The flow chart of the parametric design of the primary mirror is shown in Figure 7. Figure 8 shows the optimization results of the primary mirror using the multi-island genetic algorithm. After obtaining the set of Pareto-optimal solutions, we selected the optimal value. Table 4 shows a comparison of the results between the initial design and the optimum design. The optimal mirror surface accuracy is shown in Figure 9. In the mirror optimization, mirror optimization variables are mostly grouped according to the position of the ribs. Since the stiffness, mirror surface deformation, and mass are considered in the topology optimization of the mirror, the overall performance of the mirror can be further improved by grouping according to the topology optimization. The single objective optimization cannot improve the overall performance of the mirror, and multi-objective optimization will pose a huge challenge to optimization efficiency. Therefore, parametric design using compromise planning can not only consider multiple contradictory objectives, but also improve optimization efficiency, so the method in this paper has a certain reference value for mirror optimization.

**Table 3.** Optimal thicknesses of the lightweight ribs.

Design Variables	Domains (mm)	Initial Value (mm)	Optimum Value (mm)
ribs1	[3, 8]	5	6.4
ribs2	[3, 8]	5	3.0
ribs3	[3, 8]	5	3.2
ribs4	[3, 8]	5	3.3
ribs5	[3, 8]	5	7.4
ribs6	[3, 8]	5	4.8
ribs7	[3, 8]	5	3.4
ribs8	[3, 8]	5	3.3
ribs9	[3, 8]	5	3.6
ribs10	[3, 8]	5	4.9
ribs11	[3, 8]	5	3.1
ribs12	[3, 8]	5	7.2
ribs13	[3, 8]	5	8.0
ribs14	[3, 8]	5	4.6
ribs16	[3, 8]	5	6.9
ribs17	[3, 8]	5	8.0
ribs18	[3, 8]	5	6.8
ribs20	[3, 8]	5	4.0
ribs21	[3, 8]	5	5.2
ribs25	[3, 8]	6	4.5
ribs26	[6, 10]	8	7.7
ribs29	[6, 10]	8	6.1

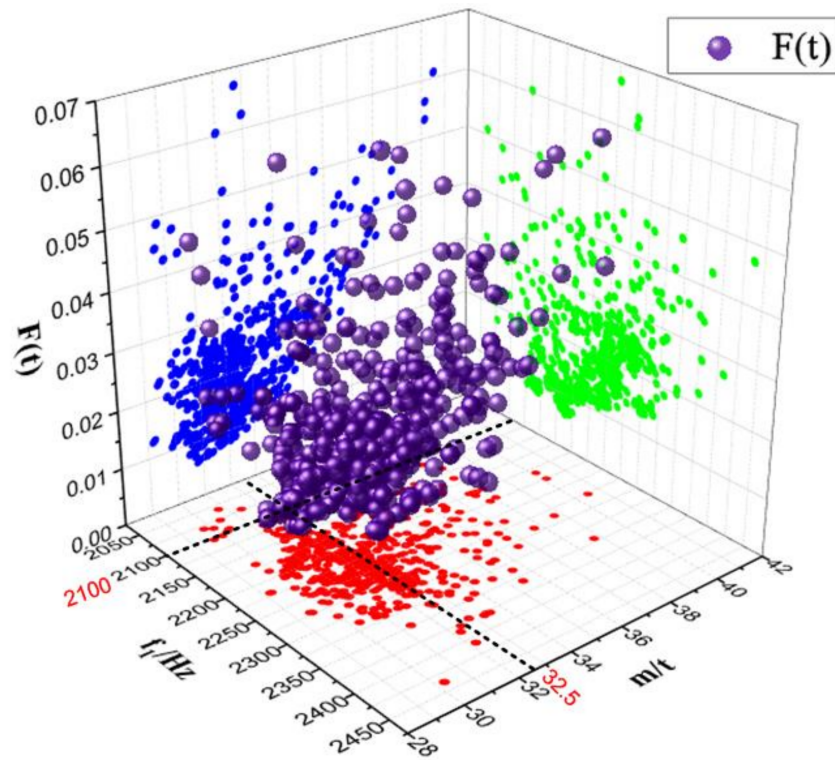


Figure 8. Design optimization results for the primary mirror.

Table 4. Results comparison of the initial and optimal design.

Response	F(t)	RMSx (nm)	RMSz (nm)	M (kg)	f <sub>1</sub> (Hz)
Initial	0.0218	2.1	5.7	33.8	2228.2
Optimization	0.00632	1.8	5.1	30.9	2188.2
Deign difference	−71%	−14.3%	−10.5%	−8.5%	−1.8%

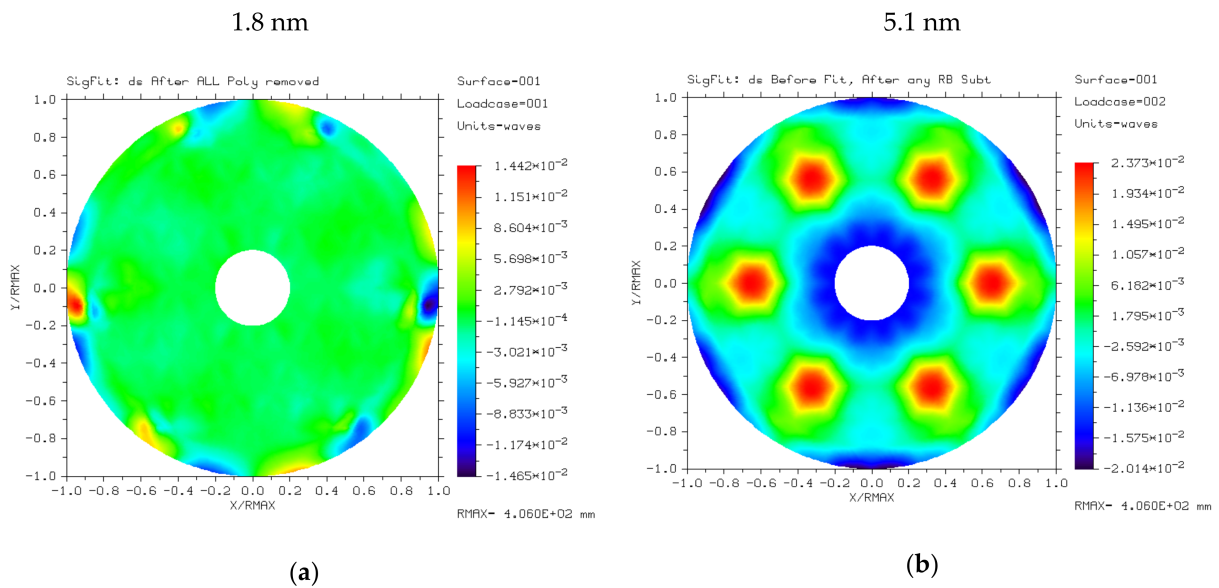


Figure 9. Result of mirror surface accuracy after optimization: (a) gravity vertical to the optical axis (RMSx) and (b) gravity parallel to the optical axis (RMSz).

#### 4. Conclusions

In this paper, the parametric design method of the primary mirror based on topology optimization is proposed. The topology optimization of the primary mirror was used as the basis for grouping lightweight ribs. The parametric design based on the compromise programming method can solve the contradictory multi-objective problem of primary mirror contradiction. This method can realize automated update iteration design, which greatly reduces the design cycles. Compared with the primary mirror structure designed based on traditional experience, the mass of the primary mirror designed by the proposed method was reduced from 33.8 kg to 30.9 kg, which meets the design requirement of less than 32.5 kg; the RMS<sub>x</sub> and RMS<sub>z</sub> were reduced by 14.3% and 10.5%, respectively; and the fundamental frequency was reduced by only 1.8%. The performance of the primary mirror met the requirements. The results show that the parametric design method based on topology optimization is effective for the design of the balloon-borne telescope's primary mirror. The parametric design method based on topology optimization provides an efficient technical mean and an engineering reference for the primary mirror of balloon-borne telescopes and space cameras in the future.

It should be noted that although our parametric design of the primary mirror based on topology optimization achieved good results in this work, the actual mirror built with this method may not achieve the optimized performance due to manufacturing errors. Hence, subsequent research work will manufacture the primary mirror for further experimental verification.

**Author Contributions:** Project administration, W.Z. and X.W.; methodology, F.L. and H.Z.; writing—original draft, F.L.; writing—review and editing, W.L., G.L., and W.Z. All authors have read and agreed to the published version of the manuscript.

**Funding:** This research was funded by the Strategic Priority Research Program of Chinese Academy of Sciences, grant number XDA17010205.

**Institutional Review Board Statement:** Not applicable.

**Informed Consent Statement:** Not applicable.

**Data Availability Statement:** The study did not report any data.

**Conflicts of Interest:** The authors declare no conflict of interest.

#### References

1. Stephens, H. Near-space. *Air Force Mag.* **2005**, *88*, 36–40.
2. Allen, E.H. The case for near space. *J. Aerospace Am.* **2006**, *44*, 31–34.
3. Pascale, E.; Ade, P.A.; Bock, J.J.; Chapin, E.L.; Chung, J.; Devlin, M.J.; Dicker, S.; Griffin, M.; Gundersen, J.O.; Wiebe, D.V. The balloon-borne large aperture submillimeter telescope: BLAST. *Astrophys. J.* **2008**, *681*, 400–414. [[CrossRef](#)]
4. Hargrave, P.C.; Ade, P.A.R.; Bock, J.J.; Chapin, E.L.; Chung, J.; Devlin, M.J.; Dicker, S.; Griffin, M.; Gundersen, J.O.; Halpern, M.; et al. BLAST—The Balloon-borne Large Aperture Sub-millimeter Telescope. In Proceedings of the 2007 Joint 32nd International Conference on Infrared and Millimeter Waves and the 15th International Conference on Terahertz Electronics, Cardiff, UK, 2–9 September 2007; Institute of Electrical and Electronics Engineers (IEEE): Los Alamitos, CA, USA, 2007; pp. 596–597.
5. Walker, C.; Kulesa, C.; Bernasconi, P.; Eaton, H.; Rolander, N.; Groppi, C.; Kloosterman, J.; Cottam, T.; Lesser, D.; Wolfire, M.; et al. The Stratospheric THz Observatory (STO). *Proc. SPIE Int. Soc. Opt. Eng.* **2010**, *7733*, 54–58.
6. Solanki, S.K.; Riethmüller, T.L.; Barthol, P.; Danilovic, S.; Deutsch, W.; Doerr, H.P.; Feller, A.; Gandorfer, A.; Germerott, D.; Lecinski, A.; et al. The second flight of the SUNRISE balloon-borne solar observatory: Overview of instrument updates, the flight, the data, and first results. *Astrophys. J. Suppl. Ser.* **2017**, *229*, 2. [[CrossRef](#)]
7. Nakano, T.; Sakamoto, Y.; Yoshida, K.; Kuwahara, T.; Shoji, Y.; Taguchi, M.; Yamamoto, M.; Takahashi, Y. The balloon-borne telescope system for optical observation of planets. *2010 IEEE/SICE Int. Symp. Syst. Integr.* **2010**, 236–241. [[CrossRef](#)]
8. Barthol, P.; Gandorfer, A.; Solanki, S.K.; Schüssler, M.; Chares, B.; Curdt, W.; Deutsch, W.; Feller, A.; Germerott, D.; Schmidt, E.; et al. The Sunrise Mission. *Sol. Phys.* **2011**, *268*, 1–34. [[CrossRef](#)]
9. Catanzaro, B.; Brooks, T.; Johnson, W.; O'Connor, B.; Woodruff, R.; Edwards, R.; Racine, E.; Paganini, L.; Eliot, Y.; Gorius, N.; et al. "STOP modeling in support of 1-meter aperture balloon based telescope." *Astronomical Telescopes and Instrumentation*. Austin: SPIE. 2018. Available online: <https://www.spiedigitallibrary.org/conference-proceedings-of-spie/10705/2312312/STOP-modeling-in-support-of-a-1-meter-aperture-balloon/10.1117/12.2312312.full> (accessed on 27 May 2021).

10. Lee, J.H.; Park, K.-S.; Youn, S.-K. Lightweight mirror design method using topology optimization. *Opt. Eng.* **2005**, *44*, 053002. [[CrossRef](#)]
11. Hu, R.; Liu, S.; Li, Q. Topology-optimization-based design method of flexures for mounting the primary mirror of a large-aperture space telescope. *Appl. Opt.* **2017**, *56*, 4551. [[CrossRef](#)] [[PubMed](#)]
12. Qu, Y.; Jiang, Y.; Feng, L.; Li, X.; Liu, B.; Wang, W. Lightweight Design of Multi-Objective Topology for a Large-Aperture Space Mirror. *Appl. Sci.* **2018**, *8*, 2259. [[CrossRef](#)]
13. Li, Z.; Chen, X.; Wang, S.; Jin, G. Optimal design of a  $\Phi 760$  mm lightweight SiC mirror and the flexural mount for a space telescope. *Rev. Sci. Instrum.* **2017**, *88*, 125107. [[CrossRef](#)]
14. Liu, G.; Guo, L.; Wang, X.; Wu, Q. Topology and parametric optimization based lightweight design of a space reflective mirror. *Opt. Eng.* **2018**, *57*, 075101. [[CrossRef](#)]
15. Jiang, P.; Zhou, P. Optimization of a lightweight mirror with reduced sensitivity to the mount location. *Appl. Opt.* **2020**, *59*, 3799–3805. [[CrossRef](#)]
16. Xiao, D.; Zhang, H.; Liu, X.; He, T.; Shan, Y. Novel steel wheel design based on multi-objective topology optimization. *J. Mech. Sci. Technol.* **2014**, *28*, 1007–1016. [[CrossRef](#)]
17. Qiao, J.; Xu, F.; Wu, K.; Zhang, S.; Liu, Y. Multi-Objective Topological Optimization of an Electric Truck Frame Based on Orthogonal Design and Analytic Hierarchy Process. *IEEE Access* **2020**, *8*, 140923–140935. [[CrossRef](#)]
18. Meng, Q.; He, F.; Zhao, W.; Wang, K.; Yang, L.; Dong, J.; Wang, X. The Overview of the Planetary Atmospheric Spectral Telescope (PAST) in the Scientific Experimental System in Near-Space (SENSE). *ISPRS Int. Arch. Photogramm. Remote Sens. Spat. Inf. Sci.* **2019**, *XLIII-2/W13*, 1419–1423. [[CrossRef](#)]
19. Zhou, P.; Zhang, D.; Liu, G.; Yan, C. Development of space active optics for a whiffletree supported mirror. *Appl. Opt.* **2019**, *58*, 5740–5747. [[CrossRef](#)] [[PubMed](#)]
20. Yoder, P.R. *Opto-Mechanical Systems Design*, 3rd ed.; CRC Press: Boca Raton, FL, USA, 2006; pp. 503–506.
21. Tcherniak, D. Topology optimization of resonating structures using SIMP method. *Int. J. Numer. Methods Eng.* **2002**, *54*, 1605–1622. [[CrossRef](#)]
22. Buhl, T. Simultaneous topology optimization of structure and supports. *Struct. Multidiscip. Optim.* **2002**, *23*, 336–346. [[CrossRef](#)]
23. Ortigosa, R.; Ruiz, D.; Gil, A.; Donoso, A.; Bellido, J. A stabilisation approach for topology optimisation of hyperelastic structures with the SIMP method. *Comput. Methods Appl. Mech. Eng.* **2020**, *364*, 112924. [[CrossRef](#)]
24. Kihm, H.; Yang, H.-S. Design optimization of a 1-m lightweight mirror for a space telescope. *Opt. Eng.* **2013**, *52*, 091806. [[CrossRef](#)]
25. Hu, J.N.; Dong, J.H.; Zhou, P.W. Parametric design of flexure supporting for optical space remote sensor primary mirror. *Acta Opt. Sin.* **2016**, *36*, 297–304.
26. Iqbal, T.; Wang, L.; Li, D.; Dong, E.; Fan, H.; Fu, J.; Hu, C. A general multi-objective topology optimization methodology developed for customized design of pelvic prostheses. *Med. Eng. Phys.* **2019**, *69*, 8–16. [[CrossRef](#)] [[PubMed](#)]
27. Teimouri, M.; Asgari, M. Multi-objective BESO topology optimization for stiffness and frequency of continuum structures. *Struct. Eng. Mech.* **2019**, *72*, 181–190.
28. Liu, C.; Zhu, H.; Dong, R.; Zhou, S.; Huang, L. Sensitivity Analysis and Optimal Design of a Linear Magnetic Gear for Direct-Drive Wave Energy Conversion. *IEEE Access* **2019**, *7*, 73983–73992. [[CrossRef](#)]
29. Nurunnabi, M.; Roy, N.K.; Hossain, E.; Pota, H.R. Size Optimization and Sensitivity Analysis of Hybrid Wind/PV Micro-Grids- A Case Study for Bangladesh. *IEEE Access* **2019**, *7*, 150120–150140. [[CrossRef](#)]
30. Sin, G.; Gernaey, K.V. Improving the Morris method for sensitivity analysis by scaling the elementary effects. *Comput. Aided Chem. Eng.* **2009**, *26*, 925–930. [[CrossRef](#)]
31. Li, Y.; Liu, W.; Zhang, X.; Yan, C.; Gu, Z. Optimized design of high-mode main support structure for airborne spectrometer. *Opt. Precis. Eng.* **2019**, *27*, 1783–1792. [[CrossRef](#)]